

Dispersion Measurements of P Waves and their Implications for Mantle Q_p

R. J. R. DEVILEE,¹ J. TRAMPERT,¹ and H. PAULSSEN¹

Abstract— We analyze the anelasticity of the earth using group delays of P -body waves of deep (> 200 km) events in the period range 4–32 s for epicentral distances of 5–85 degrees. We show that Time Frequency Analysis (*TFA*), which is usually applied to very dispersive surface waves, can be applied to the much less dispersive P -body waves to measure frequency-dependent group delays with respect to arrival times predicted from the *CMT* centroid location and *PREM* reference model. We find that the measured dispersion is due to: (1) anelasticity (described by the P -wave quality factor Q_p), (2) ambient noise, which results in randomly distributed noise in the dispersion measurements, (3) interference with other phases (triplications, crustal reverberations, conversions at deep mantle boundaries), for which the total dispersion depends on the amplitude and time separation between the different phases, and (4) the source time function, which is dispersive when the wavelet is asymmetrical or contains subevents. These mechanisms yield dispersion ranging in the order of one to 10 seconds with anelasticity responsible for the more modest dispersion. We select 150 seismograms which all have small coda amplitudes extending to ten percent of the main arrival, minimizing the effect of interference. The main P waves have short durations, minimizing effects of the source. We construct a two-layer model of Q_p with an interface at 660 km depth and take Q_p constant with period. Our data set is too small to solve for a possible frequency dependence of Q_p . The upper mantle Q_1 is 476 [299–1176] and the lower mantle Q_2 is 794 [633–1064] (the bracketed numbers indicate the 68 percent confidence range of Q_p^{-1}). These values are in-between the *AK135* model (KENNETT *et al.*, 1995) and the *PREM* model (DZIEWONSKI and ANDERSON, 1981) for the lower mantle and confirm results of WARREN and SHEARER (2000) that the upper mantle is less attenuating than *PREM* and *AK135*.

Key words: Attenuation, body waves, Time Frequency Analysis, Q .

Introduction

An anelastic medium changes the shape of waves that travel through it. On a global scale, teleseismic S - and P -body waves have been used to assess the anelasticity by analyzing the waveforms. This can be done in the time domain by waveform fitting (CHOY and CORMIER, 1986; DZIEWONSKI and STEIM, 1982), however since anelasticity is a frequency-dependent effect, this can be more directly observed using amplitude spectra (ROTH *et al.*, 1999; GAO, 1997; WARREN and

¹ Department of Earth Sciences, Utrecht University, PO Box 80021, 3508 TA Utrecht, The Netherlands. E-mail: jeannot@geo.uu.nl

SHEARER, 2000), both amplitude and phase spectra (BHATTACHARYYA *et al.*, 1996), or group arrival times (CORREIG and VILA, 1994) which are related to the phase.

The effect of anelasticity on a P -body waveform can be expressed in terms of the quality factor, Q_p . Group arrival times have only a second-order sensitivity to Q_p (MITCHELL, 1998), but they are less sensitive to focussing effects of earth structure than amplitudes and provide constraints on the waveform that are practically independent (if we measure them in a finite frequency band) of those from amplitudes.

A robust way to measure group arrival times is provided by the method of Time Frequency Analysis (TFA). TFA has been developed to measure group arrival times of surface waves (DZIEWONSKI and HALES, 1972). TFA provides an alternative to the method used by CORREIG and VILA (1994), who characterized the group arrival times by the first maximum of band-pass filtered signals. TFA also applies filters to the seismogram, but relates group arrival times to the maximum of the envelopes of the filtered signals.

TFA of body waves is different from its application in surface wave studies, namely, (1) body waves are analyzed at short periods, whereas surface waves are usually analyzed at longer periods, (2) body waves are much less dispersive, with dispersion of about 1 s, whereas surface waves show tens of seconds of dispersion, e.g., WU and LEVSHIN (1994), and (3) their recordings often contain a sequence of separate waveforms (the coda), whereas fundamental mode surface waves often present an isolated waveform. This means that we have to re-assess the reliability of the group arrival times which we obtain.

The main purpose of this paper is to see the extent to which TFA is applicable to body waves. While CONG *et al.* (2000) have applied TFA to measure dispersion of the first swing of regionally recorded P waves, we will use information from the complete waveforms at teleseismic distances. We give an overview of the method and examine its sensitivity to different aspects of P recordings such as noise, the presence of other phases besides the direct P -wave arrival and the source time function. Then we examine the constraints that dispersion measurements of P put on a simple two-layer model of the P -wave quality factor Q_p .

Theory of Time Frequency Analysis

TFA and its application have been described in detail by DZIEWONSKI and HALES (1972). Here we summarize the theory and properties of the method.

To decompose a seismogram $u(t)$ in time and frequency, we use Gaussian bandpass filters around central frequencies f_0 of the form:

$$W(f, f_0) = c_1 \exp\left(-\frac{(f - f_0)^2}{2\sigma_f^2}\right). \quad (1)$$

The constant c_1 is not important for our applications. For real signals, amplitudes and phases at negative frequencies do not add independent information compared to that given at positive frequencies. Therefore, and for mathematical convenience, the filter width σ_f must be chosen such that

$$W(f, f_0) \simeq 0 \quad \text{for } f < 0, \quad (2)$$

at each frequency f_0 . Since a Gaussian function is nonzero everywhere, equation(2) is only approximate.

Applying a filter $W(f, f_0) + W(f, -f_0)$ to a signal yields a bandpassed signal; applying $2W(f, f_0)$ yields a complex signal $\tilde{u}(t, f_0)$, comprising the bandpassed signal as the real part and its Hilbert transform as the imaginary part. The impulse response of the Gaussian bandpass filter (equation (1)) is:

$$w(t, f_0) = c_2 \exp\left(-\frac{t^2}{2\sigma_t^2} - i2\pi f_0 t\right), \quad (3)$$

where

$$\sigma_t = \frac{1}{2\pi\sigma_f}, \quad (4)$$

and c_2 is some scaling factor. Equation (3) defines the Morlet wavelet, which is sometimes used in Wavelet Analysis (CHAKRABORTY and OKAYA, 1995). Equation (4) shows that the resolution obtainable in the time domain is inversely proportional to that in the frequency domain.

The impulse response (equation (3)), and hence also the filtered signal, are modulated by a harmonic wave, which can be removed by using $|\tilde{u}|$, the envelope of the filtered signal. DZIEWONSKI and HALES (1972) showed that the maximum of $|\tilde{u}|$ corresponds to the group arrival time, if phase and amplitude are linear functions of frequency within the frequency band, i.e., all Fourier components interfere constructively in the time domain. In case the signal is dispersive, the group arrival times are a function of f_0 .

Equation (2) implies that the filters we use should be narrow at low frequencies, but can be wider at higher frequencies. The choice $\sigma_f = \alpha f_0$ yields best time resolution if second and higher order terms in the phase are not important (CARA, 1973); this is a reasonable assumption since we are interested in measuring slowly varying dispersion due to Q_p . TFA now has one free tuning parameter, namely α . Its value should be set subjective to noise conditions and dispersiveness of the waveform of interest.

A sampling strategy should provide some degree of independence between measurements at different frequencies f_0 . If we would choose equidistant sampling with frequency, the filters which increase in width with f_0 are nearly identical for subsequent samples at high frequencies; similarly, if we would choose an equidistant

sampling with period, the filters at very large periods are nearly identical. The least bias occurs when filters at subsequent frequencies have the same relative amount of overlap, that is, are centered at frequencies $f_{j+1} = f_j + \gamma\sigma_{f,j}$. Given that the filter has width $\sigma_{f,j} = \alpha f_j$ around f_j , valid frequencies are $f_{j+1} = (1 + \gamma\alpha)f_j$. This yields an exponentially increasing series of frequencies,

$$f_j = f_0(1 + \gamma\alpha)^j, \quad (5)$$

at which we will filter the seismogram and estimate group arrival times; f_0 is the frequency at $j = 0$.

Concluding, with *TFA* we measure a physical quantity, the group arrival time, but obtain a smoothed image of the true dispersion.

On the Origin of the Dispersion

TFA consists of convolving a Gaussian time window with a signal and any seismic energy that arrives within the window is used for the group arrival estimate.

An application of *TFA* to a seismogram is shown in Figures 1a and 1b. The envelope $|\tilde{u}|$ is contoured and the group delays $\tau(f_0)$ (relative to the *CMT* solution (DZIEWONSKI *et al.*, 1981) are found as a function of frequency by tracing the maxima, indicated by circles.

In Figure 1a we find different dispersion curves associated with different waveforms in the seismogram, which merge at long periods (*P* and *pP* around 50 s period and *pP* and *PP* around 60 s period) due to decreasing time resolution with period. In Figure 1b we observe a trend which may be associated with dispersion of the *P* wave and slight oscillations in the measured dispersion which result from interference between arrivals that are so closely spaced that these cannot be separated in our period range.

The dispersion observed in Figures 1a and 1b is the result of anelastic dispersion of *P*, of the dispersiveness of the source time function, of the interference between different phases, and of ambient noise. These issues are addressed separately in this section.

Ambient Noise

Ambient noise is always present in seismograms. To examine its effect on measurements of group arrival times, we apply *TFA* to seismograms containing a delta pulse and different realizations of white noise (with a uniform probability of taking a value between -1 and $+1$) for different values of the *S/N* ratio. We define the *S/N* ratio at each frequency as the ratio between the amplitude of the envelope at the group arrival time and the largest maximum present in the remainder of the envelope.

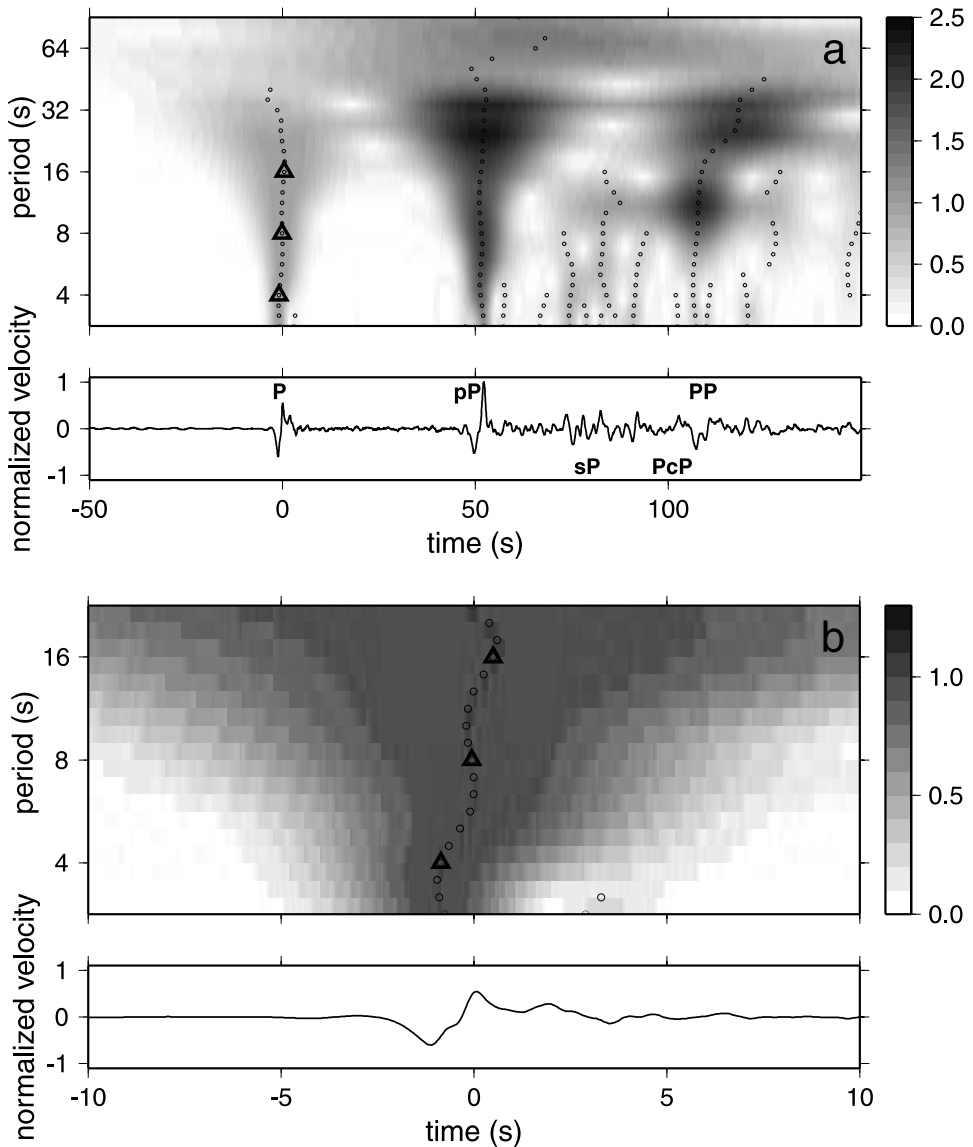


Figure 1

TFA (with filter width scale factor $\alpha = 0.3$) applied in two different period ranges to recordings of a *P* wave at station *YAK* for event 02-20-1998, M_b 5.8, with centroid located at (36.5N, 70.9E) at a depth of 243.7 km. (a) Shows interference at long periods, (b) shows interference at short periods. The epicentral distance is 44° . Envelopes of seismograms filtered around different periods form a surface as a function of time and period. At each period, envelopes are scaled by the value of the maximum associated with the *P* wave. The location of relatively strong maxima of the envelope is indicated by circles, which define the group delays associated with the strongest phases. The seismograms are shown for normalized velocity in the lower frame: these have been lowpassed using a second order Butterworth filter with a corner frequency of 0.5 Hz. Measurements used for inversion are shown by triangles.

Figures 2a and 2b show the decrease in resolution of group arrival times at 1 s period if we decrease the scale factor α or decrease the S/N ratio. The noise in the group arrival times increases with decreasing filter width σ_f due to the decrease in time resolution. Figure 3 shows the increase in standard deviation (as determined from 100,000 of such noise realizations) of the group arrival times with period, for synthetic signals with different S/N ratios. The filtering operation is linearly scalable at each period and therefore uncertainty in group arrival times increases proportionally with period. At large periods, however, we have few samples within the frequency band, resulting in less reliable noise statistics and hence in more scatter. The distribution of group arrival times is symmetric around the expected arrival time, hence, ambient noise does not introduce a bias.

White noise has spectral amplitudes proportional to \sqrt{T} for a window of length T . Thus, for analysis of a P waveform contaminated with noise, increasing σ_t results in a decrease of the S/N ratio if σ_t exceeds the window within which most of the energy of the P waveform is contained. In the case of slightly dispersed P waves, most energy is contained in the first cycle, hence, $2\sigma_t$ (note that σ_t is the *half* width) should be proportional to the period of interest, i.e., $\alpha = 1/\pi \sim 0.3$.

Concluding, random noise in a seismogram does not introduce a bias into our measurements of group arrival time, but introduces an uncertainty that depends on the choice of filter width and period.

Interference between Arrivals

The P wave is followed by a series of phases containing crustal reverberations, surface reflections (pP , sP) (e.g., Figs. 1a and b), and triplications at epicentral

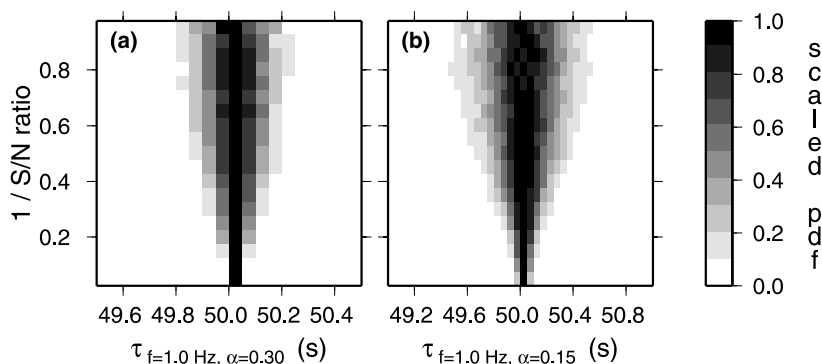


Figure 2

Distributions of group arrival times $\tau(f_0 = 1 \text{ Hz})$ obtained using *TFA* with filter width scale factor $\alpha = 0.3$ (a) and $\alpha = 0.15$ (b), for signals containing a delta pulse at 50 s and superposed white noise. The S/N ratio is given by the ratio of the amplitude of the envelope at the group arrival time and the maximum value in the surrounding ambient noise. 100,000 random realizations of the signal were analyzed. Note that the uncertainties of group arrival times in (b) are about twice as large as in (a).

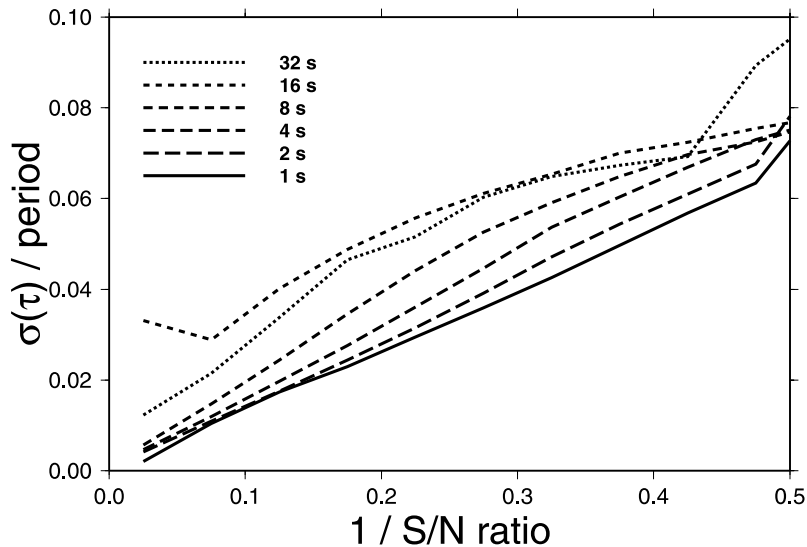


Figure 3

We applied *TFA* with $\alpha = 0.3$ to simulated recordings of delta pulses with different amounts of white noise. The S/N ratio is defined as in Figure 2. 100,000 realizations of the noise were analyzed in each case. We show the standard deviations of the scatter of values of group arrival times as a function of S/N ratio, evaluated at periods of 1, 2, 4, 8, 16 and 32 s.

distances of 15° – 30° . If a seismogram consists of a series of impulsive arrivals, bandpassing these arrivals creates a series of Gaussian-tapered harmonic waves (the impulse responses of the filter). If these waves overlap, they produce an interference pattern which depends on the amplitudes and the time interval of the phases.

For large phases like *P* and *pP* we find their mutual interference to be negligible if $2\sigma_t < \tau$, where τ is the distance between two subsequent waveforms and σ_t the halfwidth of the Gaussian. Hence, valid values for central frequencies are $f_0 > (\pi\alpha\tau)^{-1}$; if we choose $\alpha = 0.3$ (see the previous section), we have approximately $f_0 > \tau^{-1}$. On the other extreme, at frequencies $f_0 \ll \tau^{-1}$ we measure a weighted average of the group arrival times, the weight depending on the amplitudes of the waveforms involved.

Figure 1a shows a signal containing a prominent *pP* phase, arriving at $\tau = 51$ s after *P*. At periods less than τ , the group arrival times are specific to each waveform; at periods comparable to τ , interference causes substantial dispersion. The effect is strong because the two signals have similar amplitude. Such interference masks any other dispersion, including that due to Q_p . At long periods, dispersion curves merge into one average dispersion of the two waveforms. This is difficult to model, hence data in such a period range are not used in this study.

Figure 1b shows small phases arriving within about 10 s after *P*. They originate from reflections and conversions at mantle and crustal boundaries. Since the phases form a complicated coda, we cannot determine a frequency band which is free of

interference. These phases, because they only occur after the P wave and have non-random amplitudes, always contribute to the dispersion. The interference introduces an oscillatory signature into the dispersion so that we may identify cases where interference is strong. In this example however, the phases have relatively small amplitudes and the dispersion due to interference is also small.

Concluding, subsequent large phases can be analyzed at periods shorter than their separation in time. Interference of P with small phases introduces minor noise into our measurements.

Source Time Function

The shape of each arrival is the result of the source time function convolved with the response of the earth. The source time function causes dispersion if it is asymmetric in time; see Figure 4. Some source time functions consist of different subevents which produce dispersion through interference. This dispersion is small at periods that exceed the source duration, but is significant at shorter periods. Events with good signal-to-noise-ratio at periods reaching 32 s have a duration of several seconds, hence we will measure dispersion at periods of 4 s and higher.

Anelasticity

We model the effect of anelasticity by the P -wave quality factor, Q_p , which we assume is constant with period. This model yields group delays which are a linear function of log-period. An inversion would fit a linear trend in the data, with limited sensitivity to oscillations from interference. *PREM* predicts a variation of about 0.5 s of the differential group delays (relative to a reference period of 4 s) over a period range of 4–32 s (Fig. 5).

We have discussed several sources of dispersion which contribute to our measurements. In subsequent sections we invert the measurements of group delays for the quality factor Q_p only. The other forementioned effects are considered as noise, and hence we choose the data in such a way as to keep these effects to a minimum.

Measurements

Group delays

For our measurements we use vertical component *BHZ* seismograms, sampled at 20 Hz, and *LHZ* seismograms, sampled at 1 Hz, deconvolved by the instrument response to velocity. We apply *TFA* and examine the envelopes at different periods. The location of the maximum peak within a time window of 40 s centered around the predicted Centroid Moment Tensor (*CMT*) arrival time (DZIEWONSKI *et al.*, 1981; DZIEWONSKI and WOODHOUSE, 1983) yields the group delay.

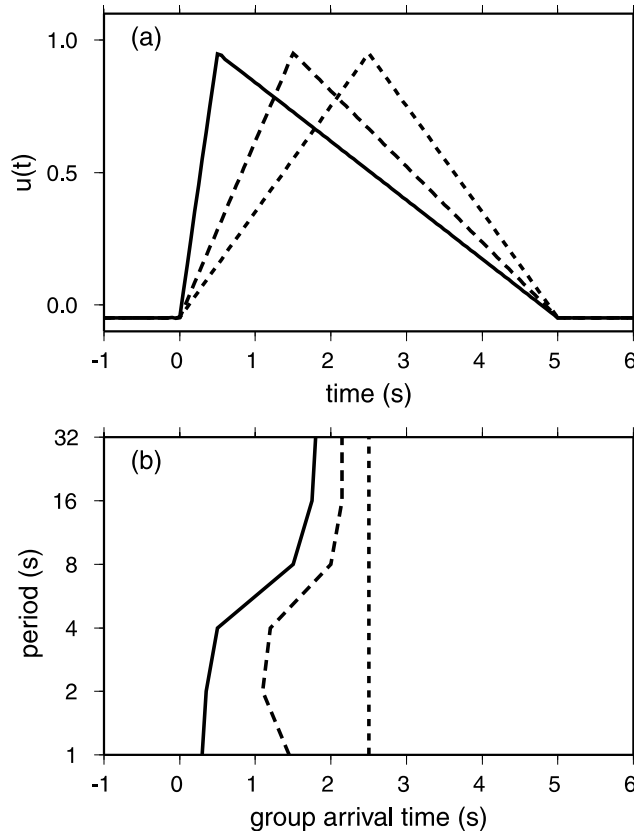


Figure 4

Dispersion of triangular waveforms intended to resemble simple source time functions from a source with a linear rise and healing time, but negligibly small fault surface. The asymmetry of a signal introduces dispersion.

We use data from 01–1990 to 09–2000, obtained from *IRIS*. The epicentral distance range is 5 to 85 degrees. A few measurements are recorded at < 30 degrees; those may include interference between upper mantle triplications. We use only deep (> 200 km) events, so that the largest phases, namely *P* and *pP*, are well separated. The period range we use is 4–32 s; 4 s is an upper limit of the source durations, and 32 s is the period above which group delays show interference with the *pP* waveform for the shallowest of the events, given that α is around 0.3. Within this period range we choose frequencies $f_j = 2^{-j}$, $j = 2, 3, 4, 5$.

We reject data in period ranges that have bad *S/N* ratio, show significant interference, or exhibit complicated *P* wave shapes. We selected 150 seismograms which have two or more acceptable group delay samples out of several thousands of seismograms which had reasonable *S/N* (> 5) ratio. The coverage of the data is

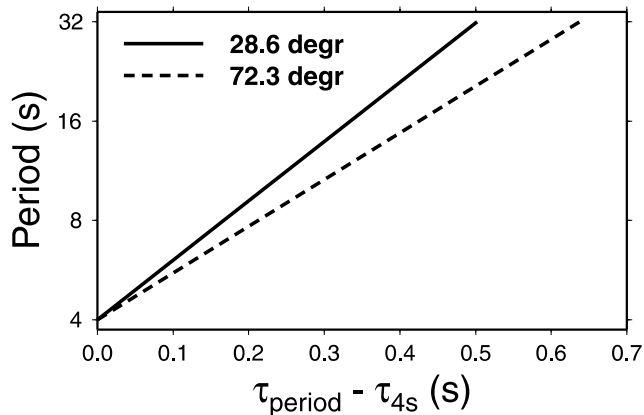


Figure 5

Dispersion of P waves calculated from the $PREM Q_p$ model (DZIEWONSKI and ANDERSON, 1981) for a source at 600 km depth and recorded at epicentral distances of 29 and 72 degrees, respectively. Differential group delays are relative to the value at 4 s period. Dispersion increases with distance.

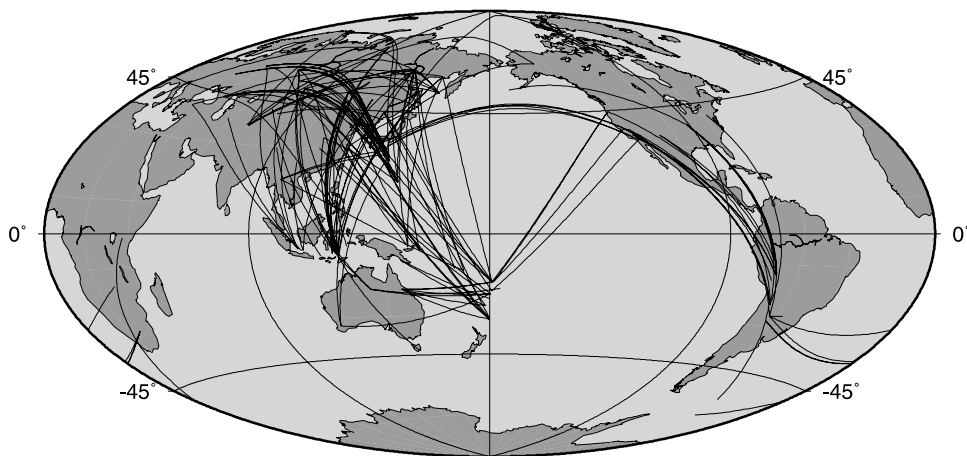


Figure 6

Coverage of event-station pairs which yield at least one differential group delay measurement. Most sources lie along the Pacific Rim where deep seismicity occurs, however some are located under southwestern Tibet. Most stations are located on continents.

shown in Figure 6. The data are most representative of structure in Eastern Asia and the Western Pacific.

Uncertainties

We measure group delays using three values of the filter scaling factor α , namely, 0.25, 0.30 and 0.35. Choosing a smaller width causes interference between P and pP

for the shallow events; a larger width means that we use a time window significantly less than one cycle, i.e., we become sensitive to details of the source. In-between, no value is unambiguously preferred over another. We use the average of these measurements, τ_i at each frequency f_i , for inversion. Their standard deviation σ_α represents the uncertainty due to α . Another source of uncertainty is due to ambient noise. We measure the S/N ratio of the recordings and use the previously established uncertainties in the group delays as a function of the S/N ratio (Fig. 3). We add the squared standard deviations, so that the total uncertainty in τ_i is now represented by the standard deviation $\sigma_i^2 = \sigma_\alpha^2 + \sigma_{\text{noise}}^2$.

Differential Group Delays

The group delays τ_i (averaged from different α) at frequencies f_i contain a frequency-dependent part due to anelastic properties of the earth, and a frequency-independent part due to elastic velocity variations in the earth. We eliminate the latter at each station by taking the average group delay at frequency f_i relative to the average group delay at another frequency f_j , i.e., by using $\Delta\tau_{ij} = \tau_i - \tau_j$. We call this the *differential group delay*. The uncertainty of the differential group delay is the sum of uncertainties of the two average group delays, i.e., $\sigma_{ij}^2 = \sigma_i^2 + \sigma_j^2$. By choosing a particular reference frequency f_j we favor a certain noise at that frequency. To obtain a fair representation of the noise, we measure differential group delays $\Delta\tau_{ij}$ for all reference frequencies j .

Observed differential group delays correspond to wide distributions, but also show a clear trend with period, indicative of the presence of dispersion (Fig. 7).

Inversion for Q_p

Inversion Theory

We define a simple model which has two layers with homogeneous Q_p , namely $Q_p = Q_1$ for $z < 660$ km and $Q_p = Q_2$ for $z > 660$ km where z denotes depth. The boundary at 660 km depth separates the upper and lower mantle, and here we expect the most significant change of Q_p with depth. We use the approximation that Q_1 and Q_2 are constant in the seismic frequency band, and express the predicted differential group delays Δs_{ij} by (BEN-MENAHEM and SINGH, 1981):

$$\Delta s_{ijk} = s_k(f_i) - s_k(f_j) = -\frac{2t_k^*}{\pi} \ln\left(\frac{f_i}{f_j}\right), \quad (6)$$

where $s_k(f_j)$ is the group arrival time in a spherically symmetric earth for ray path k . Note that high frequency energy arrives earliest. The value of t_k^* is related to Q_p by (BEN-MENAHEM and SINGH, 1981):

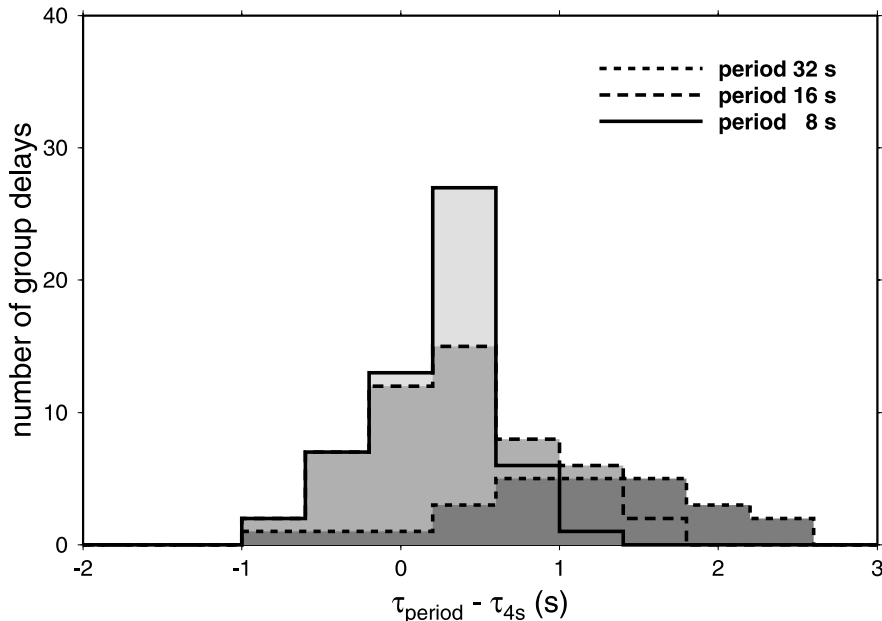


Figure 7

The distribution of the measured *P*-wave differential group delays, relative to the values at 4 s period. The distributions are wide, but are shifted which clearly indicates dispersion.

$$t_k^* = \int_0^R n_k(r) \frac{dr}{v_p(r) \sqrt{1 - (v_p(r) p_k r^{-1})^2}} \frac{1}{2Q_p(r)}, \tag{7}$$

where *R* denotes the earth’s radius, *n_k(r)* an integer giving the number of times the ray path *k* samples the earth at radius *r*, *v_p(r)* the *PREM P* velocity model of the earth (DZIEWONSKI and ANDERSON, 1981), and *p_k* the ray parameter for a spherical medium. We assume that this ray theoretical estimate of differential group delays is valid in our frequency range.

We define the misfit *E* between sets of *K* synthetics $\Delta s_{ijk}(Q_1, Q_2)$ and measurements $\Delta \tau_{ijk}$, each with *N* frequency samples, by:

$$E(Q_1, Q_2) = \sum_{k=1}^K \sum_{j=1}^N \sum_{i=j+1}^N \frac{w_{ijk}}{m \sigma_{ijk}^m} |\Delta \tau_{ijk} - \Delta s_{ijk}|^m \left[\sum_{k=1}^K \sum_{i=1}^N \sum_{j=n_1(i)}^{n_2(i)} w_{ijk} \right]^{-1}, \tag{8}$$

where *w_{ijk}* = {0, 1} indicates our confidence in the differential group delays. By normalizing *E* by the summed weights we obtain a chi-squared value. We dropped the dependence on the *Q_p* model for clarity. We use *m* = 2, i.e., the *L*² norm; the use of *m* = 1 (the *L*¹ norm) only slightly changes the results.

The data are distributed as a function of period, epicentral distance, and depth. Tests showed that weighting by these distributions hardly changes the results and hence we use a uniform weighting in the inversion.

We systematically vary Q_1^{-1} and Q_2^{-1} between 0 and 2 to obtain E . This gives us the shape of the complete misfit function.

Results

The model we use for Q_p is a constant function of frequency and should provide a robust result in the form of an estimate of average Q_p between 4 and 32 s period.

Figure 8 shows the misfit surface (equation (8)) of the data in this period range. The minimum of the misfit forms an ellipsoid valley with little variation of the misfit inside, showing a significant linear trade-off between Q_1^{-1} and Q_2^{-1} due to the poor sampling of the upper mantle by the teleseismic ray paths. The values of the misfit are large. In terms of χ^2 , we mismatch the data by about 2 standard deviations. This is due to the presence of effects of interference and the source time function in the

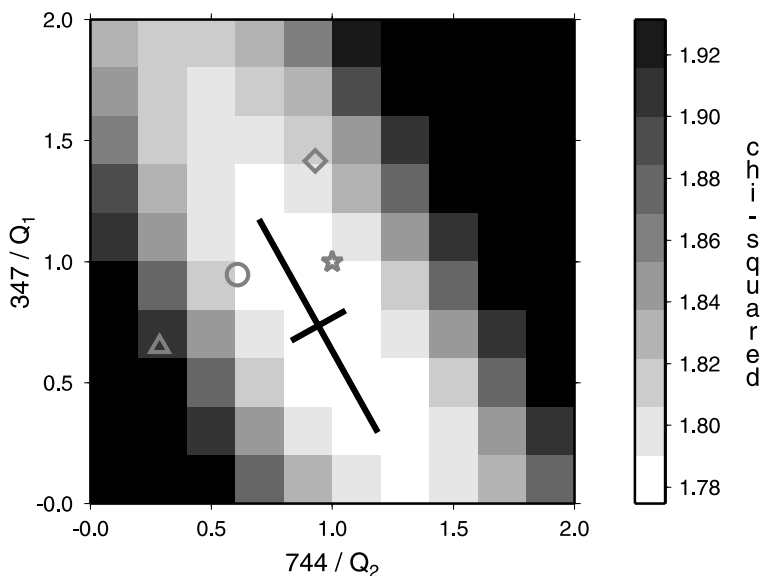


Figure 8

Misfit surface of data (equation (8) with norm $m = 2$). Q_p values of earth models *PREM* (DZIEWONSKI and ANDERSON, 1981) (star), *QL6* (DUREK and EKSTRÖM, 1996) (diamond), *AK135* (KENNETT *et al.*, 1995) (circle) and *WL* (WARREN and SHEARER, 2000) (triangle) are shown; these values are representative of the dispersion for a source at 400 km depth and a station at 50 degrees epicentral distance. The error bars indicate the root of the principle components of the cross-correlation matrix of a jackknife experiment, characterizing the distribution of optimal solutions to 500 linear inversions, each fitting a random subset of 50% of the data set. This indicates the uncertainty in the mean.

measurements of differential group delay, whose errors were not included in the inversion.

Uncertainty of the solution is determined by the available distribution of the data and their uncertainties. This is shown by the error bars which we obtain using jackknifing (EFRON, 1982; TICHELAAR and RUFF, 1989). Equations (6) and (7) pose a linear problem in Q_p^{-1} , namely $\mathbf{d} = \mathbf{G}\mathbf{q}$, where \mathbf{d} is a vector containing all measured differential group delays, and $\mathbf{q} = (Q_1^{-1}, Q_2^{-1})$. In order to obtain the optimal solution for $m = 2$, we minimize the misfit function E (equation (8)). We run 500 linear inversions using a random subset of 50% of the data and the covariance of the optimal models yields the jackknife estimate of uncertainty in the average.

We infer $Q_1^{-1} = 2.1 \pm 1.25 \cdot 10^{-3}$, yielding $Q_1 = 476$ with 68 percent probability that Q_1 is between 299 and 1176, and $Q_2^{-1} = 1.26 \pm 0.32 \cdot 10^{-3}$, yielding $Q_2 = 794$ with 68 percent probability that Q_2 is between 633 and 1064. Note that the misfit function of Q_p^{-1} is symmetric around the mean, which maps into an asymmetric uncertainty estimate of Q_p .

Conclusion

We used Time Frequency Analysis to measure group arrival times. This method has been applied to very dispersive surface waves, but we showed that it can also be applied to the much less dispersive P body waves. The dispersion is expressed as frequency-dependent group delays which provide information about the earth which is independent of amplitude data. The measurements depend on the filter width; variation around its optimal value indicates the uncertainties in the measurement due to noise.

The measurements represent the effects of attenuation, interference and the source time function on the shape of the P waveform. The dispersion due to interference depends on the size and sign of the amplitudes of the phases following P , and is easily identified due to its oscillatory nature.

We used 150 high quality dispersion measurements of P body waves to constrain Q_p (the P -wave quality factor) in the mantle. We used a model of Q_p that is constant with period in order to obtain robust results. The simple model contained two layers with a boundary at 660-km depth. The inverse of upper mantle Q_p (Q_1^{-1}) and lower mantle Q_p (Q_2^{-1}) trade off linearly. The valley of acceptable misfit lies in-between the values of the *AK135* model (KENNETT *et al.*, 1995) and the *PREM* model in the lower mantle. The optimal model we find is $Q_1 = 476$ and $Q_2 = 794$, with an indication that the upper mantle is less attenuating than *PREM* or *AK135*, in agreement with findings of WARREN and SHEARER (2000).

Acknowledgements

This research was funded by the *Geodynamics Research Institute* at *Utrecht University*. *CMT* solutions are from the *Harvard Catalogue* and waveforms are provided by *IRIS* [<http://www.iris.washington.edu>]. Plots are made with the *Generic Mapping Tool* (WESSEL and SMITH, 1999).

REFERENCES

- BEN-MENACHEM, A. and SINGH, S. J., *Seismic Waves and Sources* (Springer Verlag, New York, NY, United States, 1981).
- BHATTACHARYYA, J., MASTERS, G., and SHEARER, P. (1996), *Global Lateral Variations of Shear-wave Attenuation in the Upper Mantle*, *J. Geophys. Res.* *101*, 22,273–22,289.
- CARA, M. (1973), *Filtering of Dispersed Wavetrains*, *Geophys. J. R. Astr. Soc.* *33*, 65–80.
- CHAKRABORTY, A. and OKAYA, D. (1995), *Frequency-time Decomposition of Seismic Data Using Wavelet-based Methods*, *Geophysics* *60*, 1906–1916.
- CHOY, G. L. and CORMIER, V. F. (1986), *Direct Measurement of the Mantle Attenuation Operator from Broadband *P* and *S* Waveforms*, *J. Geophys. Res.* *91*, 7326–7342.
- CONG, L., MEJIA, J., and MITCHELL, B. J. (2000), *Attenuative Dispersion of *P* Waves in and near the New Madrid Seismic Zone*, *Bull. Seismol. Soc. Am.* *90*, 679–689.
- CORREIG, A. M. and VILA, J. (1994), *Measurement of Body-wave Dispersion and Estimation of Related Attenuation from Broadband Stations*, *Phys. Earth Planet. Int.* *84*, 193–206.
- DUREK, J. J. and EKSTRÖM, G. (1996), *A Radial Model of Anelasticity Consistent with Long-period Surface-wave Attenuation*, *Bull. Seismol. Soc. Am.* *86*, 144–158.
- DZIEWONSKI, A. M. and HALES, A. L., *Numerical analysis of dispersed seismic waves*. In *Methods in Computational Physics*, Volume 11, *Seismology: Surface Waves and Earth Oscillations* (ed. Bolt B.A.) (Academic Press, New York, 1972) pp. 39–85.
- DZIEWONSKI, A. M. and ANDERSON, D. L. (1981), *Preliminary Reference Earth Model*, *Phys. Earth Planet. Int.* *25*, 297–356.
- DZIEWONSKI, A. M., CHOU, T.-A., and WOODHOUSE, J. H. (1981), *Determination of Earthquake Source Parameters from Waveform Data for Studies of Global and Regional Seismicity*, *J. Geophys. Res.* *86*, 2825–2852.
- DZIEWONSKI, A. M. and WOODHOUSE, J. H. (1983), *An Experiment in Systematic Study of Global Seismicity: Centroid-moment Tensor Solutions for 201 Moderate and Large Earthquakes of 1981*, *J. Geophys. Res.* *88*, 3247–3271.
- DZIEWONSKI, A. M. and STEIM, J. M. (1982), *Dispersion and Attenuation of Mantle Waves through Waveform Inversion*, *Geophys. J. R. Astr. Soc.* *70*, 503–527.
- EFRON, B., *The Jackknife, the Bootstrap and Other Resampling Plans* (Society for Industrial and Applied Mathematics, Philadelphia, Pennsylvania, 1982).
- GAO, S. (1997), *A Bayesian Nonlinear Inversion of Seismic Body-wave Attenuation Factors*, *Bull. Seismol. Soc. Am.* *87*, 961–970.
- KENNETT, B. L. N., ENGDAHL, E. R., and BULAND, R. (1995), *Constraints on Seismic Velocities in the Earth from Traveltimes*, *Geophys. J. Int.* *122*, 108–124.
- MITCHELL, B., *Regional Studies of Crustal Anelasticity Using Body and Surface Waves* (Fourth Workshop on Three-dimensional Modelling of Seismic Waves Generation, Propagation and their Inversion, ICTP, Trieste, 1998).
- ROTH, E. G., WIENS, D. A., DORMAN, L. M., HILDEBRAND, J., and WEBB, S.C. (1999), *Seismic Attenuation Tomography of the Tonga-Fiji Region Using Phase Pair Methods*, *J. Geophys. Res.* *104*, 4795–4809.
- TICHELAAAR, B. W. and RUFF, L. J. (1989), *How Good are Our Best Models? Jackknifing, Bootstrapping and Earthquake depth*, *EOS, Transactions* *70*, pp. 593 and 605–606.

- WARREN, L. M. and SHEARER, P. M. (2000), *Investigating the Frequency Dependence of Mantle Q by Stacking P and PP Spectra*, *J. Geophys. Res.* *105*, 25,391–25,402.
- WESSEL, P. and SMITH, W. H. F., *The Generic Mapping Tools (GMT) Version 3.2, Technical Reference and Cookbook* (SOEST/NOAA, 1999).
- WU, F. T. and LEVSHIN, A. (1994), *Surface-wave Group Velocity Tomography of East Asia*, *Phys. Earth Planet. Int.* *84*, 59–77.

(Received January 9, 2002, accepted March 29, 2002)



To access this journal online:
<http://www.birkhauser.ch>
